

Performance assessment of pitch-type wave energy converter in irregular wave conditions on the basis of numerical investigation

Sunny Kumar Poguluri¹, Dongeun Kim² and Yoon Hyeok Bae^{*1}

¹Department of Ocean System Engineering, Jeju National University, Jeju, South Korea

²Multidisciplinary Graduate School program for Wind Energy, Jeju National University, Jeju, South Korea

(Received November 22, 2021, Revised January 20, 2022, Accepted February 8, 2022)

Abstract. In this paper, a pitch-type wave energy converter (WEC-rotor) is investigated in irregular wave conditions for the real sea testing at the west coast of Jeju Island, South Korea. The present research builds on and extends our previous work on regular waves to irregular waves. The hydrodynamic characteristics of the WEC-rotor are assessed by establishing a quasi-two-dimensional numerical wave tank using computational fluid dynamics by solving the Reynolds-averaged Navier–Stokes equation. The numerical solution is validated with physical experiments, and the comparison shows good agreement. Furthermore, the hydrodynamic performance of the WEC-rotor is explored by investigating the effect of the power take-off (PTO) loading torque by one-way and two-way systems, the wave height, the wave period, operational and high sea wave conditions. Irrespective of the sea wave conditions, the absorbed power is quadratic in nature with the one-way and two-way PTO loading systems. The power absorption increases with the wave height, and the increment is rapid and mild in the two-way and one-way PTO loading torques, respectively. The pitch response amplitude operator increases as the wave period increases until the maximum value and then decreases. For a fixed PTO loading, the power and efficiency are higher in the two-way PTO loading system than in the one-way PTO loading system at different wave periods.

Keywords: absorbed power; efficiency; numerical simulation; one-way and two-way PTO loading; wave energy converter

1. Introduction

The projected positive vibes around the world toward the development of renewable energy in recent years has attracted and increased the implementation of policies toward carbon neutrality as the case is in South Korea. The mid- and long-term goals of the national and local government of South Korea require renewable energy infrastructure to be 100% carbon-free and to achieve speedy carbon neutrality, one among the prominent focus is wave energy converter (WEC) devices. Several types of WEC device have been developed over several decades to capture the energy of sea waves, but very few have been successfully deployed for testing. Among the existing WECs, Salter's duck (a WEC-rotor) is one of the promising devices, mainly employing pitch response to capture the wave

*Corresponding author, Professor, E-mail: yh.bae@jejunu.ac.kr

power, and reportedly has a high efficiency (Salter 1974, Skyner 1987). The WEC-rotor is an example of a terminator type, which pitches up and down about a fixed axis (see Fig. 1). The WEC-rotor responds by changing its position according to the incoming wave dynamic pressure and the varying hydrostatic pressure both in phase converts the oscillating motion to rotational motion. The present research extends our previous work on regular waves to irregular waves (see Poguluri *et al.* 2019, Kim *et al.* 2019). The primary focus is the numerical investigation of a WEC-rotor suitable for the design wave conditions selected for the west coast of Jeju, South Korea.

In the initial stages of WEC development, studies based on regular waves play an important role in understanding the physics of a WEC device. A wide range of potential modelling techniques are available, such as numerical, and experimental methods, for the wide range of WEC concepts and the different sizes and operational principles (Bhattacharyya and McCormick 2003, Folley 2016, Pecher 2017, Falnes 2002). However, laboratory measurements are expensive, and parametric study is difficult to conduct. Numerical solutions are the alternative option. The well proven and established numerical hydrodynamic formulations based on the linear approach are the most general and acceptable throughout a device's operational regime (Folley 2016). Skyner (1987), Pizer (1994), and Poguluri and Bae (2018) studied based on linear potential flow theory on WEC-rotor. Although the incoming wave is linear, the response of the WEC-rotor is nonlinear, limiting the usage of linear theory. To overcome this limitation, some of the researchers adopted weakly nonlinear analysis while others performed nonlinear time domain analysis. In the former method, the nonlinear external restoring and damping moments are included in the linear solution (Poguluri *et al.* 2019, Kim *et al.* 2019). To obtain the wave loads and wave induced motions accurately, nonlinear time domain analysis is essential for a safe, reliable, and cost-effective WEC design. Poguluri *et al.* (2020), Ko *et al.* (2021), and Ha *et al.* (2021) conducted an investigation based on computational fluid dynamics (CFD) using Star-ccm+ and OpenFOAM. A quasi-2D numerical wave tank (NWT) was used, and its important numerical settings and effect on WEC-rotor interaction with regular waves was studied based on the wave generation; wave absorption, grid aspect ratio, turbulent model, high-resolution interface capturing scheme (HRIC), and interface momentum dissipation (IMD) were applied to the model scale and extended to the WEC-rotor prototype by Poguluri *et al.* (2020). The numerical results are consistent with the experimental results. Ko *et al.* (2021) performed CFD investigation to obtain an optimum power take-off (PTO) loading torque using OpenFoam when the WEC-rotor is exposed to regular and irregular waves. PTO loading is implemented by applying a constant load torque opposite to the response of the WEC-rotor. Uni- and bi-directional loading torques were tested in both the regular and irregular wave conditions, and the results show that the uni-directional PTO loading torque is more efficient than the bi-directional loading torque. Ha *et al.* (2021) conducted a CFD investigation on the WEC-rotor to understand its nonlinear behavior response to regular waves. Their experimental results were compared with the CFD simulations. Their results indicate that as the wave height increases, the response of the WEC-rotor is influenced by the wave runup and slamming.

Pecher *et al.* (2012) experimentally studied a WEC-rotor, which is placed on a floating platform, whose power estimation was tested for the wide range of sea wave conditions. They discussed dependency of the significant wave height (H_s), the peak period (T_p), and the PTO loading torque (τ_{pto}). They reported that T_p is the more dependent than H_s in extracting the wave power. Linear and constant τ_{pto} were optimized for different sea state conditions. The linear τ_{pto} shows a significantly better performance than the constant PTO loading. Generally, the WEC-rotor is largely efficient within a narrow bandwidth near the resonant frequency. To extend the range of the resonant

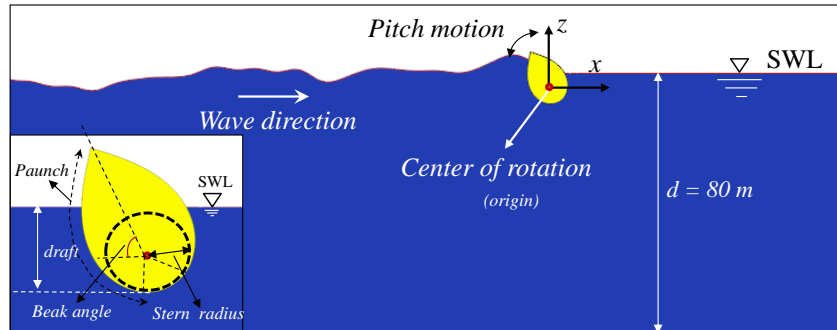


Fig. 1 Schematic geometric details of the WEC-rotor and the adopted coordinate system

frequency, a negative stiffness in the WEC-rotor system was analyzed by Peretta *et al.* (2015). Laboratory tests have been carried out in regular and irregular waves with a maximum wave height of 6 m and a wave period ranging from 5 s to 9 s at prototype scale. A comparison was also performed between numerical simulations and experimental test results and revealed a reasonably good agreement. The overall performance has improved by 60% if a negative spring is included in the WEC-rotor. Ko *et al.* (2021) investigated the performance of the WEC-rotor by evaluating the two types of PTO loading torque. The extracted power was reported based on the H_s range from 0.5 m to 1.25 m for a fixed T_p of 5.50 s. The extracted power can be maximized by selecting the τ_{pto} in the range of 9–14 kNm. Many works have been published in the context of the WEC-rotor in regular waves, but studies based on irregular waves are limited. This allows researchers to explore even further and investigate the challenges and uncertainties involved in the power assessment of the WEC-rotor in irregular waves. To address important issues, the present study aims to investigate the interaction of the WEC-rotor with irregular waves in operation and high sea wave conditions using CFD with Star-ccm+. Furthermore in the present study, PTO loading torque is implemented similar to Coulomb damping, which replicates the hydraulic system in a full scale machine. It is possible to achieve controllability by maintaining a constant damping torque with a pressurized hydraulic circuit (two-way PTO loading system, $\pm\tau_{pto}$) that changes sign with angular velocity. Using the hydraulic piston in the hydraulic circuit, the piston exerts a constant moment, and the WEC is prevented from moving until the external force exceeds the applied PTO load torque, which corresponds to the hydraulic oil pressure times the area of the piston. One can achieve limited controllability by τ_{pto} to be zero and allowing WEC to move freely under the influence of external forces and exerts τ_{pto} whenever necessary, either during positive or negative angular velocity of the WEC oscillation (one-way control) in the opposite direction. Such a Coulomb type of damping (one- and two-way τ_{pto} systems) is an advantage both in practical and theoretical viewpoints. In addition, such a control mechanism allows by considering nonlinear effects (António 2007, 2008).

The rest of this paper is structured as follows. In Section 2, the overview of the physical problem and the geometric details are presented. Section 3 presents the numerical model based on the Reynolds-averaged Navier–Stokes (RANS) equation, including the computational setup. Numerical validation and parametric sensitivity analysis were conducted to determine the optimal conditions on the basis of the operational wave conditions, the PTO loading torques (one-way and two-way), the wave height, the wave period, and high sea wave conditions, and the results are discussed in Section 4. Finally, the conclusion is presented in Section 5.

Table 1 Wave period ratios ($\frac{T_e}{T_z}$, $\frac{T_p}{T_z}$, $\frac{andTe}{T_p}$) for JONSWAP spectrum based on specified γ

JONSWAP (γ)	$\frac{T_e}{T_p} = 0.8255 + 0.03852\gamma - 0.005537\gamma^2 + 0.0003154\gamma^3$ and $\frac{T_z}{T_p} = 0.6673 + 0.05037\gamma - 0.006230\gamma^2 + 0.003341\gamma^3$		
	$\frac{T_e}{T_z}$	$\frac{T_p}{T_z}$	$\frac{T_e}{T_p}$
1	1.22	1.40	0.87
3.3	1.18	1.29	0.92

2. Overview of the physical problem

A WEC-rotor was selected for testing at the western coast of Jeju, South Korea at a water depth (d) of 80 m and the schematic detail of the physical problem is shown in Fig. 1. The mean Joint North Sea Wave Project (JONSWAP) was used to describe the site-specific sea wave conditions and is expressed as

$$S_J(\omega) = (1 - 0.287 \cdot \ln(\gamma)) \frac{5}{16} (H_s^2 \omega_p^4) \omega^{-5} \exp\left(-\frac{5}{4} \left(\frac{\omega}{\omega_p}\right)^{-4}\right) \cdot \gamma \exp\left(-0.5 \left(\frac{\omega - \omega_p}{\sigma \omega_p}\right)^2\right) \quad (1)$$

where $\omega_p = (2\pi)/(T_p)$ represents the angular spectral peak frequency, γ is the non-dimensional peak shape parameter, and σ is the non-dimensional peak shape parameter. If $\omega \leq \omega_p$, then $\sigma = 0.07$; else, $\sigma = 0.09$. The present work aims to simulate and test under operational and high sea state conditions. The chosen non-dimensional peak shape parameter and the corresponding energy wave period (T_e), zero-crossing period (T_z), and peak period (T_p) and their ratios are provided in Table 1 (DNV 2014).

The geometric modelling of the WEC-rotor is presented in our previous publications (Poguluri *et al.* 2018) and the primary components of the model and prototype-1 are tabulated in Table 2. In real-time testing, the WEC-rotor is modified to improve its structural stability, and the reinforcement through additional frames increases the total weight. To maintain increased weight, the modified rotor (prototype-2) is designed by retaining the most important properties, such as the natural period and the external geometric parameters similar with those of prototype-1, as tabulated in Table 2. The undamped natural frequency of the WEC-rotor is given by

$$T = 2 \times \pi \sqrt{\frac{I_{yy} + I_{add}}{M_{res}}} \quad (2)$$

where I_{yy} is the moment of inertia about y -axis, I_{add} is the added moment of inertia, and M_{res} is the hydrostatic restoring moment.

The experiments were performed with the WEC-rotor in a 3D wave basin at the Research Institute of Medium and Small (RIMS) shipbuilding in South Korea. The WEC-rotor model was placed in the wave basin (28 m \times 22 m \times 2.5 m) at the middle (lengthwise and widthwise). Operational design wave conditions were selected and compared with the CFD simulations. For the

Table 2 Principal particulars of model and prototype scale dynamic properties of the WEC-rotor

Description	Units	Model (1:11)		Prototype - 1		Prototype - 2	
Mass	Kg	13.65		21345.35		56490.41	
CoG	<i>m</i>	(-0.0931, 0.0, 0.0998)		(-0.8935, 0, 1.0169)		(-0.3377, 0.0120, 0.0871)	
		CoR	CoG	CoR	CoG	CoR	CoG
I_{xx}		0.7037	0.5678	106900.64	84825	285294.25	284857.96
I_{yy}	$kg \cdot m^2$	0.7479	0.4937	117369.20	78375.91	212272.77	205401.18
I_{zz}		0.6853	0.5670	98481.69	81564.06	217467.53	211015.89
Draft		0.3275		3.6		3.6	
Stern radius	<i>m</i>	0.1820		2.0		2.0	
Width		0.4550		5.0		5.0	
Undamped natural period	<i>s</i>	1.53		5.13		4.99	

CFD simulations, a quasi-2D NWT was used to generate the desired experimental wave conditions. The WEC-rotor exposed to the incoming irregular waves and the adopted coordinate system for the simulations are shown in Fig. 1. The origin of the earth-fixed coordinate system coincides with the center of rotation of the WEC-rotor, and the wave travels from the negative x -axis to the positive x -axis.

3. Numerical method

The authors of this paper previously performed a thorough numerical investigation of the WEC-rotor and its interaction on the basis of regular waves (Poguluri *et al.* 2020). Most of the parameters from the previous study (Poguluri *et al.* 2020) were retained unless otherwise specified as the numerical settings were deemed to be the most accurate and suitable for the analysis. For the baseline setup, the grid aspect ratio, the time step, the wave generation and damping regions, and the numerical schemes (second-order discretization schemes in both time and space) were determined as shown in Table 3. Two immiscible fluids, water, and air, are treated as incompressible Newtonian fluids, and the flow past the WEC-rotor can be described by the following governing equations known as the RANS and continuity equations

$$\underbrace{\frac{\partial(u_i)}{\partial t}}_{\text{local acceleration}} + \underbrace{\frac{\partial(u_i u_j)}{\partial x_j}}_{\text{advection}} = \underbrace{-\frac{1}{\rho} \frac{\partial p}{\partial x_i}}_{\text{pressure gradient}} + \underbrace{\frac{\partial}{\partial x_i} \left[(\nu + \nu_t) \left(\frac{\partial u_i}{\partial x_j} + \frac{\partial u_j}{\partial x_i} \right) \right]}_{\text{diffusion}} + \underbrace{g_j}_{\text{gravity}} \quad (3)$$

$$\frac{\partial u_i}{\partial x_i} = 0 \quad (4)$$

where u_i and u_j are the velocity field averages over time ($i, j = 1, 2$), p is the pressure, and g is the gravitational acceleration. A laminar model was used for the simulations, where the eddy viscosity (ν_t) was ignored. The local fluid density and viscosity (ν) are defined by the volume of fluid (VOF) model.

$$\rho = (1 - \alpha_{water})\rho_{air} + \alpha_{water}\rho_{water} \quad (5)$$

$$\nu = (1 - \alpha_{water})\nu_{air} + \alpha_{water}\nu_{water} \quad (6)$$

where the volume fraction (α) of water can be expressed by the scalar transport equation

$$\frac{\partial \alpha_{water}}{\partial t} + \nabla (\alpha_{water} \mathbf{u}) = 0 \quad (7)$$

To maintain a sharp additional interface, schemes, such as HRIC and IMD, were included.

3.1 Computational setup

The baseline computational setup is shown in Fig. 2. The list of boundary conditions is provided in Table 3 along with the exact location of the boundaries. The present simulations are expected to generate reflected waves at both ends and to reduce a wave forcing zone at the negative x -axis, and 200-m wide wave damping zone at positive x -axis were adopted. The variation in the xz -plane was considered in the simulations, and the vertical side walls were treated under the symmetric boundary conditions. The flow field was initialized with the corresponding JONSWAP spectrum as tabulated in Section 2. The grid size with reference to the base size (h) was used to describe the different regions with targeted anisotropic cells as very fine, fine, or coarse (Fig. 2). The cell aspect ratio in the refinement region at the very fine zone was maintained at 1:2 in the z and x directions, and a higher or equivalent cell size was allowed at the WEC-rotor and next to the overset region as shown in Table 3 and Fig. 2. Around the WEC-rotor, the effect of pressure and frictional drag predominantly existed, and the boundary layer adequately captured must be resolved for which a fine prism-layer mesh was selected. The total thickness of prism-layer of 0.1 m, which was divided into four layers, was generated from the WEC-rotor surface, and the result is a $y^+ < 3$. A classic way to control WEC is by linear damping, where the applied PTO moment is linearly proportional to the angular velocity of the WEC-rotor (τ_{pto}) given by $\tau_{pto} = -B_{pto}\omega_{wec}$ which is regarded as a simple mechanism see Fig. 3. It is fair enough to implement a Coulomb type of damping capable of exerting either zero moment or a constant moment ($\tau_{pto} = \pm\tau_0$, applied moment see Figs. 3(a) and 3(b), independent of the instantaneous angular velocity of the WEC-rotor allowing specification of moments at discrete time steps. During application of the moment, the body will remain stationary unless, or until, the hydrodynamic force on the WEC-rotor overcomes the resisting moment. Further one- and two-way τ_{pto} systems are implemented numerically in the present study and tested in irregular waves by using Eq. (8). The implementation of the one-way τ_{pto} system means, a torque is applied only during a positive angular velocity; else, the torque will be zero (Fig. 3(a)). In the case of two-way

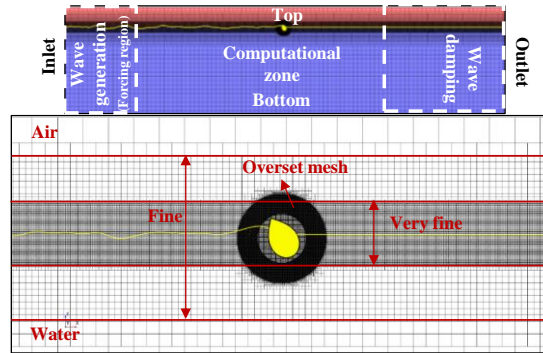


Fig. 2 Numerical domain setup: Boundary conditions and generated mesh

Table 3 Boundary conditions and mesh refinement regions with base size of $h = 4$ m

Boundary	Inlet	Velocity inlet	$x = -300$ m
	Outlet	Pressure outlet	$x = 300$ m
	Sides	Symmetric	$y = \pm 2.5$ m
	Top	Pressure outlet	$z = +20$ m
	Bottom	Wall	$z = -80$ m
Wave generation and absorption	Wave forcing zone = 100 m and Damping zone = 200 m		
Very fine region	$-300 > x < 300$ and $-2 \times H > z < 2 \times H$		$\Delta x/h = 1/10; \Delta y/h = 1/4; \Delta z/h = 1/20$
Fine region	$-300 > x < 300$ and $-4 \times H > z < 4 \times H$		$\Delta x/h = 1/5; \Delta y/h = 1/4; \Delta z/h = 1/10$
Course region	$-300 > x < 300$ and $-6 \times H > z < 6 \times H$		$\Delta x/h = 1/2; \Delta y/h = 1/4; \Delta z/h = 1/4$
WEC-rotor and overset region			$\Delta x/h = 1/40; \Delta y/h = 1/4; \Delta z/h = 1/40$
$T_p/\Delta t$			400
Pressure-velocity coupling		Semi-Implicit Method for Pressure-Linked Equations (SIMPLE)	
Iterations			10
Under-relaxation factors		Pressure = 0.2 and velocity = 0.8	
Mesh moving technique		Overset	
Time discretization		Second-order implicit backward-differencing	
Spatial discretization		Second-order upwind	
Volume meshing		Anisotropic trimmer	

τ_{pto} system the load torque is applied in both directions opposite to the pitch motion of WEC-rotor (Fig. 3(b)).

$$\tau_{pto} = \begin{cases} \begin{cases} -\tau_0 & \omega_{WEC} > 0 \\ 0 & \omega_{WEC} \leq 0 \end{cases} \text{One-way} \\ \begin{cases} -\tau_0 & \omega_{WEC} > 0 \\ 0 & \omega_{WEC} = 0 \\ +\tau_0 & \omega_{WEC} = 0 \end{cases} \text{Two-way} \end{cases} \quad (8)$$

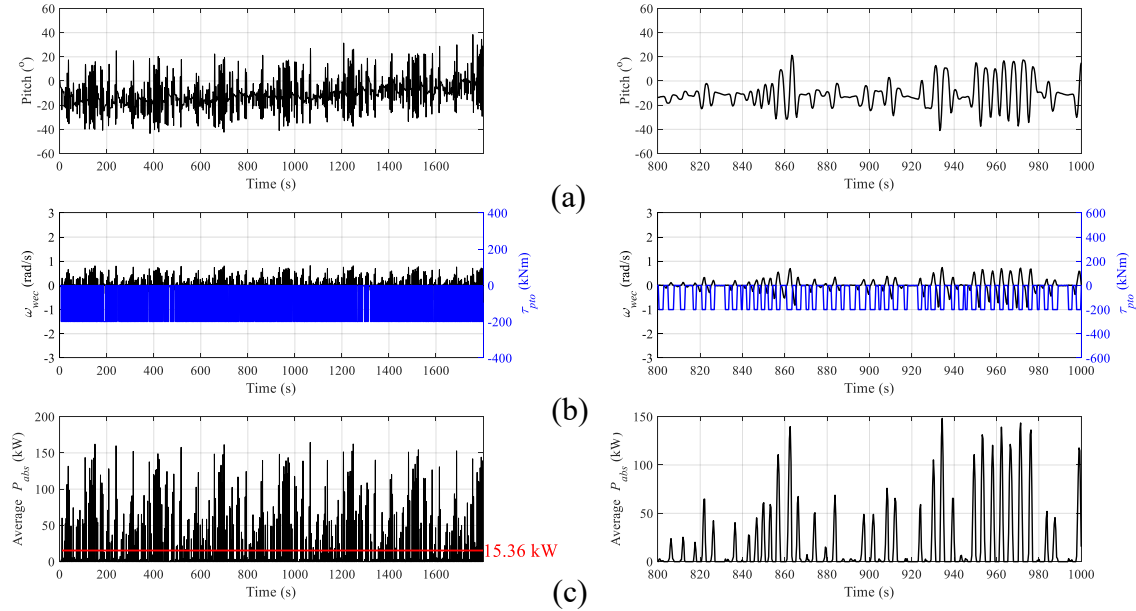


Fig. 4 Instantaneous variation of pitch response (a), angular velocity and PTO loading torque (b), and average absorbed power for the wave conditions of $H_s=1.76$ m, $T_p=4.81$ s, and $\tau_{pto}=200$ kNm

scale down model was selected as the WEC-rotor as shown in Table 2. The wave parameters were scaled to a model as H_s and T_p to 0.16 and 1.45 s, which represent the operational conditions at the western coast of Jeju Island. The average P_{abs} values of the WEC-rotor from the numerical simulations are compared with the experimental model results by extrapolating to the prototype scale.

Fig. 4 shows the instantaneous time series results based on the numerical simulations. To verify the results, the key outputs of the WEC-rotor for the power calculation were assessed by showing the instantaneous variations for a period of 1800 s. The pitch response shown in Fig. 4(a) changes within the range of -40° to $+40^\circ$. The corresponding angular velocities and the applied one-way load torque are presented in the subplots in Fig. 4(b). Generally, a discontinuous behavior is expected while changing the applied torque direction in linear models (such as Orcaflex), and to overcome such behavior a ramp function is used. This issue does not persist when the CFD implementation is adopted as shown in Fig. 4(b). One-way τ_{pto} was smoothly implemented and by applying at positive angular velocity. Fig. 4(c) shows the absorbed power for the selected range whose average value is marked with a red line. The estimated average absorbed power and efficiency from the numerical simulations were 15.36 kW and 48.51%, respectively, and the efficiency can be expressed in percentage as average $P_{abs}/(P_w \times width) \times 100$. The experimental measurements are 16.43 kW and 52.22%, showing an approximately 7% difference from the numerical results. The WEC-rotor prototype-2 will be considered for the rest of the analysis unless otherwise specified.

4.2 Effect of PTO loading torque at operating wave conditions

The effect of τ_{pto} was determined on the basis of the prototype-2 WEC-rotor model. The

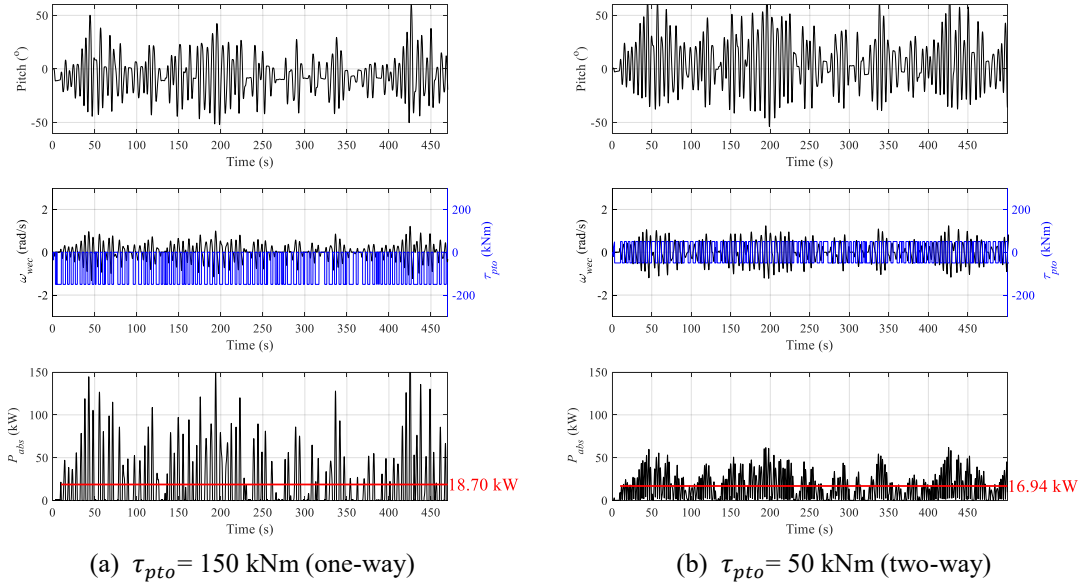


Fig. 5 Instantaneous variation of pitch response, angular velocity and PTO loading torque, and average absorbed power for the wave conditions of $H_s=2.0$ m, and $T_p=6.65$ s, for different ways of PTO loading system

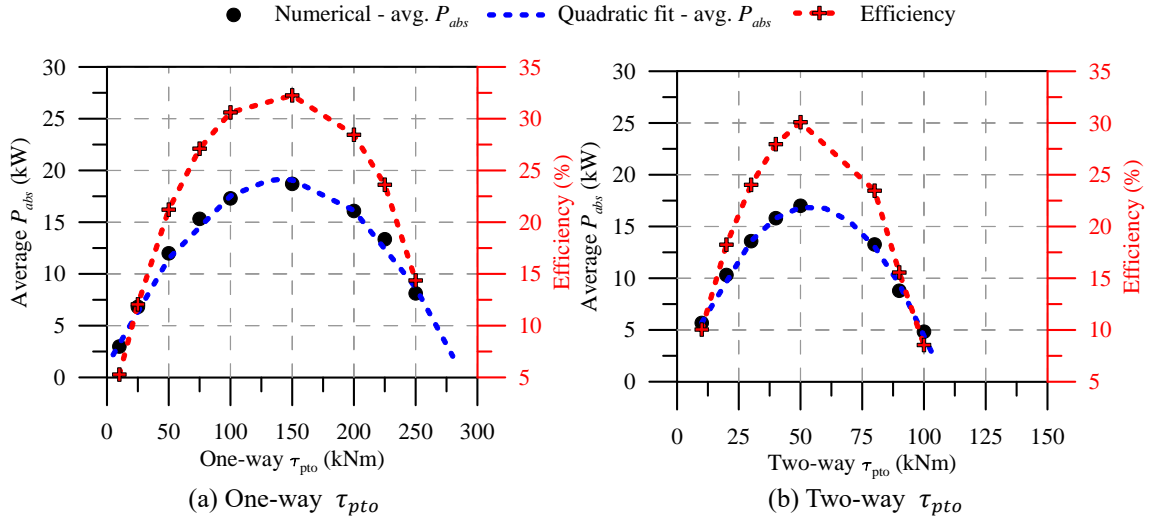


Fig. 6 Variation of average absorbed power and efficiency for a fixed wave conditions of $H_s=2.0$ m, and $T_p=6.65$ s, for different ways of PTO loading system

testing involved two types of PTO loading systems: one corresponds to the one-way system, and the other corresponds to the two-way system. The optimal PTO values for both systems were determined. The testing was carried out numerically for a wide range PTO values, and the irregular wave characteristics were set as follows: $T_p=6.65$ s, $H_s=2.0$ m, and $\gamma = 1.0$. For the one-way and two-

Table 4 Calculated pitch response, average absorbed power, and efficiency with different wave heights for one-way and two-way τ_{pto} systems

	H_s (m)	Pitch ($^\circ$)	Average P_{abs}	Efficiency (%)
One-way	1	23.71	4.49	31.77
	1.5	48.23	7.93	24.94
	2	54.83	11.55	20.44
Two-way	1	14.47	2.64	18.68
	1.5	17.84	9.48	29.82
	2	32.95	16.52	29.22

way systems, load torques from 10 kNm to 200 kNm and 10 kNm to 80 kNm were simulated and are presented in Fig. 6 as the absorbed power and efficiency. A typical time series at peak maximum average absorbed power for a fixed value of τ_{pto} is shown in Fig. 5 for both the one-way and two-way systems. The subplots of Fig. 5 show the variables that were used in the power calculation along with the pitch response of the WEC-rotor.

In both ways of PTO loading, the absorbed power increases with the load torque and reaches the maximum value. Then, the power decreases as the load torque continues to increase (Fig. 6). The range of the applied load torque is higher for the one-way system than for the two-way system. This result indicates that the susceptibility of the absorbed power is moderate with the increase of the applied load torque in the one-way system and relatively stronger in the two-way system. To see the trend followed by the absorbed power for the WEC-rotor, a curve is fitted to the pair of points (τ_{pto} and averaged P_{abs}) by using polynomial of second order denoted in blue dotted line (Fig. 6). The goodness of fit of the curve is decided based on the R -squared value called the coefficient of determination (see Fig. 6). For the one-way and two-way systems, the R -squared value has been obtained as 0.9946 and 0.9998, respectively, indicating that the absorbed power is quadratic in nature with the PTO loading system irrespective of the type of loading systems.

4.3 Effect of wave height

The motion response and the power absorption are desired to be independent of the incident wave height for WEC device. To investigate, Table 4 gives the mean pitch response ($^\circ$), absorbed power (kW), and efficiency in percentage for three different wave heights $H_s = 1.0$ m, 1.5 m, and 2.0 m. and the other parameters are $\tau_{pto} = 50$ kNm, $T_p = 6.65$ s, and $\gamma = 1.0$ using one-way and two-way systems. In both τ_{pto} systems, the average absorbed power increases with the significant wave height; the increment is rapid in the two-way system and gradual in the one-way system. This behavior probably manifests when the WEC-rotor is subjected with high steepness, apart from the first order wave loads, higher-order waves would be more affective. Large wave elevations difference at the front and rear sides leading to high wave runup and slamming forces. Such violent motion around the WEC-rotor tends to break the waves and interaction becomes nonlinear. It can be envisaged that, the complex behavior around the WEC-rotor must be suppressed largely in the two-way system than by the one-way and noticeable in the Figs. 7 (a) and 7(b) (top). Furthermore, at a

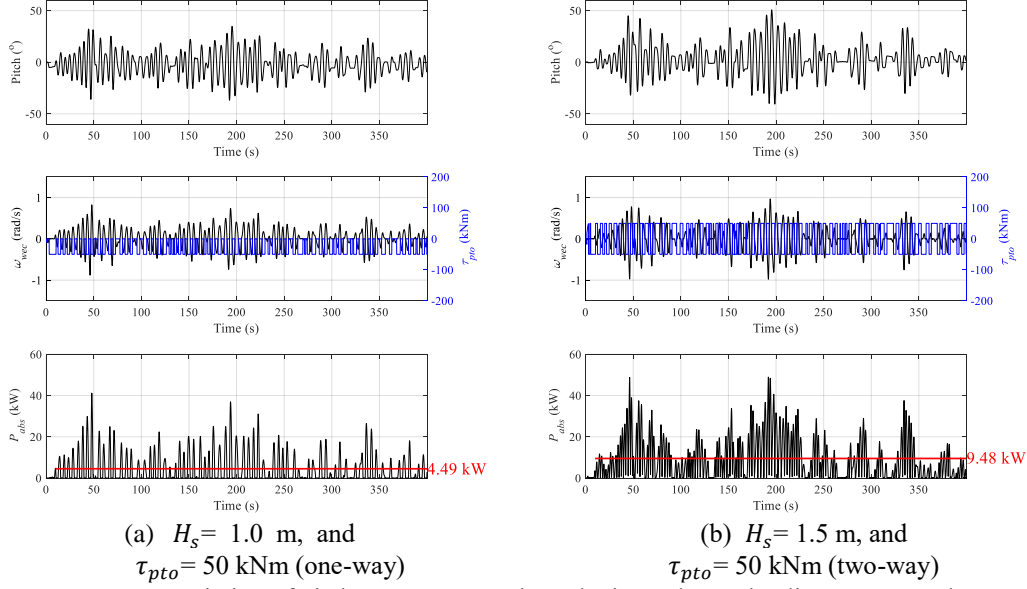


Fig. 7 Instantaneous variation of pitch response, angular velocity and PTO loading torque, and average absorbed power for the different wave height where $T_p = 6.65$ s

fixed τ_{pto} , the efficiency increases with the wave height in the two-way system and decreases in the one-way system. Fig. 7 presents the typical instantaneous pitch, the angular velocity, applied PTO torque and the average absorbed power using one-way and two-way systems.

4.4 Effect of wave period

Fig. 8(a) shows the pitch response amplitude operator (RAO) of the WEC-rotor for the range of the zero crossing wave periods ($T_z = 3.25, 3.75, 4.75, 5.25, 6.25$ s). The pitch RAO is normalized with the wave height and presented in rad/m (Fig. 8(a)). Within the considered wave period range, when the short-wave periods ($T_z = 3.25$ and 3.75 s) interacted with the WEC-rotor, the WEC-rotor did not move in phase with the surface waves, and the motion amplitude was the smallest among the wave periods. In both ways of PTO loading, the peak was at the design wave period ($T_z = 4.75$ s), but the magnitude of pitch RAO was higher in one-way PTO loading than in two-way PTO loading system. The absorbed power and efficiency are shown in Fig. 8(b). At a fixed PTO loading torque system ($\tau_{pto} = 50$ kNm), two-way τ_{pto} extracted higher power than one-way τ_{pto} at all wave periods. The maximum absorbed power was at the wave period of $T_z = 4.75$ s, where the highest efficiency was at $T_z = 3.75$ s. Furthermore, irrespective of the wave period considered, the efficiency of the two-way PTO loading torque system is greater than that of the one-way PTO loading torque system.

4.5 Effect of PTO loading torque in high sea wave conditions

The effect of the PTO loading system during high sea wave conditions also plays an equal and

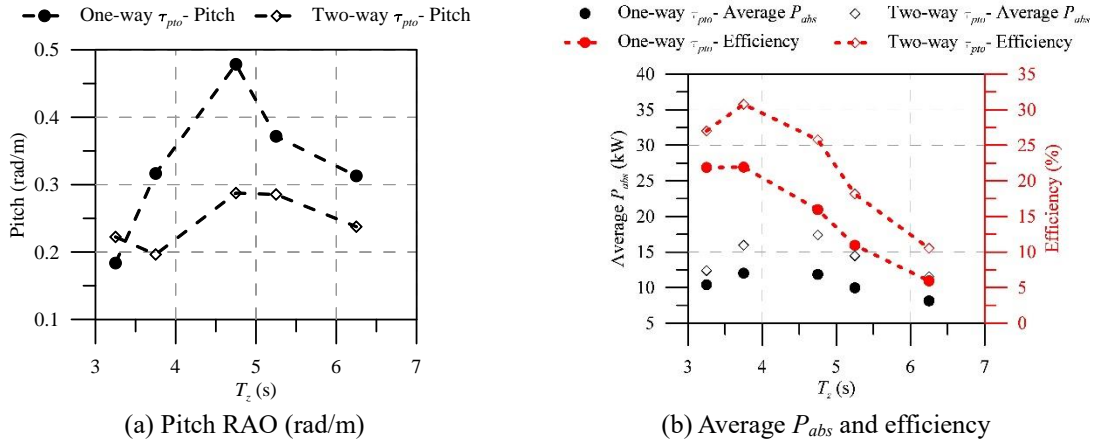


Fig. 8 Variation of pitch RAO, average absorbed power and efficiency for different wave periods (T_z) of $H_s=2.0$ m, and $\tau_{pto}=50$ kNm

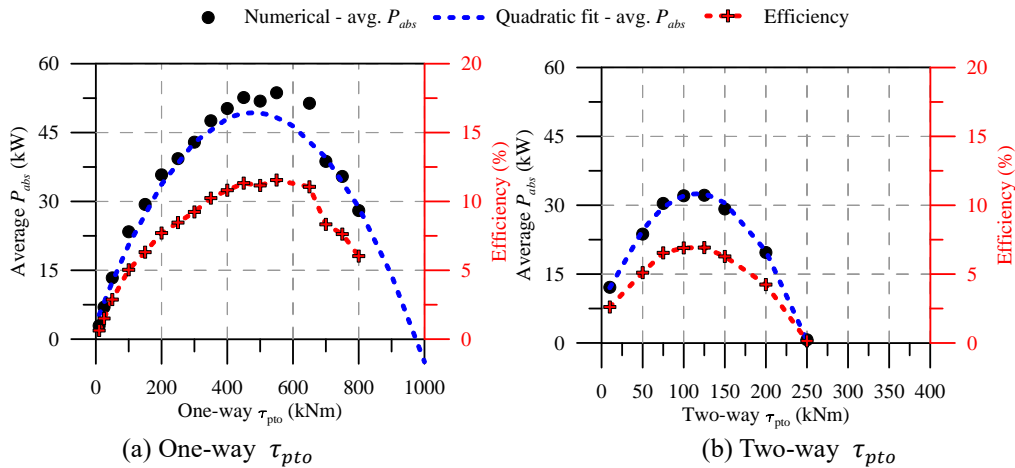
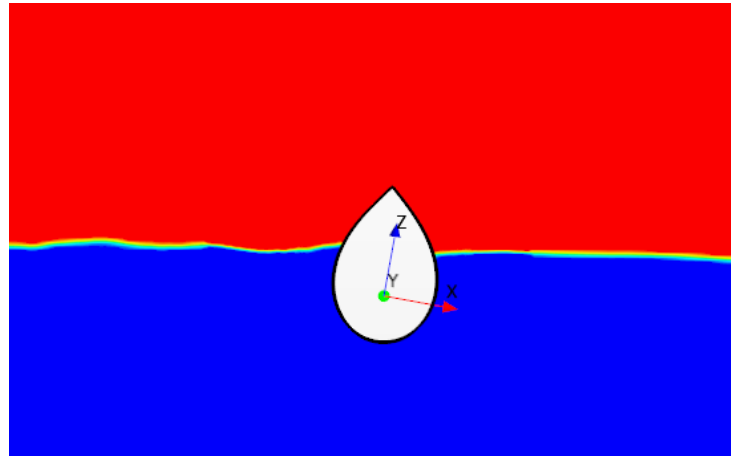


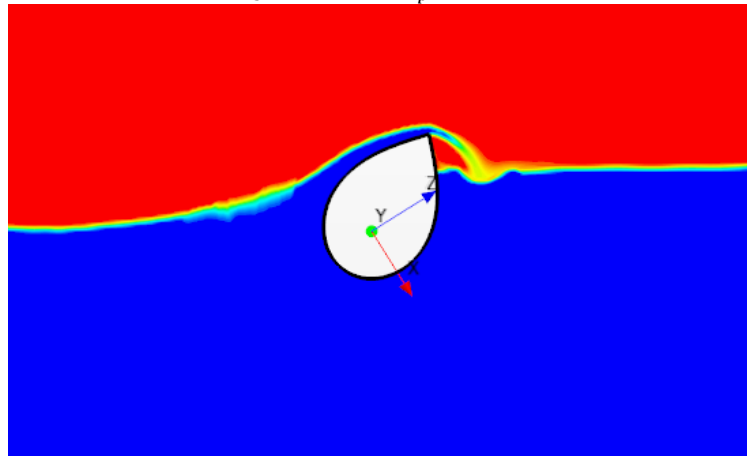
Fig. 9 Variation of average absorbed power and efficiency for an high sea wave condition of $H_s=4.75$ m, and $T_p=9.69$ s, for different ways of PTO loading system in high sea wave

challenging role in the power absorption by the WEC-rotor. The performance of the WEC-rotor in an high sea wave condition was investigated numerically and assumed to be influenced by storms on the basis of the testing location. For the investigation, the following high sea wave conditions were assumed to be defined by the JONSWAP spectrum: $H_s=4.75$, $T_p=9.69$ s, and $\gamma=3.3$. T_e and T_z are 7.51 and 10.53 s, respectively.

Fig. 9 shows that by increasing the one- and two-way τ_{pto} systems, the absorbed power follows a similar trend as that under the operation wave conditions. The power absorption is quadratic in behavior with the applied PTO loading (see blue dotted line in Fig. 9). Fig. 9 indicates the quadratic fit for both the one- and two-way τ_{pto} systems. Basically, in high sea wave conditions, the



(a) Operational wave conditions of $H_s=2.0$ m, and $T_p=4.75$ s at extreme clockwise rotation position



(a) High sea wave conditions of $H_s=4.75$ m, and $T_p=9.69$ s at extreme clockwise rotation position

Fig. 10 Flow around the WEC-rotor shown as VOF of water for operational and high sea wave conditions

absorbed power exceeded 50 kW and 32.17 kW in the one- and two-way loading systems, which are nearly three and two times higher than the operational wave conditions, respectively. The efficiency decreased by three and four times in comparison. The reduction in the efficiency of the WEC-rotor is higher than the absorbed power increment under the high sea wave condition compared to operational wave conditions. The wave energy extraction from WEC-rotor exceeded 50 kW in the one-way PTO loading system under an high sea wave condition.

For a better understanding of the physical flow interaction of the WEC-rotor and the wave, the VOF of water is presented in Fig. 10. The flow around the WEC-rotor mainly experiences profile drag, which can be further divided into the pressure and frictional drags. In addition, the WEC-rotor interaction involves wave runup, slamming, and breaking. These complex flow phenomena around the WEC-rotor are stronger for high sea wave conditions due to high incoming wave heights experienced by the WEC-rotor compared to operational wave conditions as shown in Fig. 10. Moreover, the incoming wave tries to overtop the WEC-rotor and capture it completely in high sea conditions, which is unlike in operational conditions (Fig. 10). WEC-rotors are generally equipped

with a stopper/break mechanism to prevent capsizing. In the numerical solution, a similar mechanism could be implemented by restricting it to a particular allowable angle, which was not pursued in the present study. The nonlinear effects are well noticed in both wave conditions, the slamming, breaking, and wave runup are visibly stronger and greater in the high sea conditions, resulting in decreased efficiency compared to that under operational wave conditions.

5. Conclusions

In this work, the power extraction properties of a pitch-type Salter's duck (i.e., WEC-rotor) were studied in the context of quasi-two-dimensional CFD using a NWT by generating irregular wave conditions. Incompressible Newtonian fluid with water and air were treated with the RANS equation. The motion of the WEC-rotor was captured with the overset mesh moving technique. Initially, the numerical solution was validated with the results from the laboratory experiments whose model scale parameters were extrapolated to the prototype scale for comparison. The comparison shows a good agreement between the experimental results and the numerical solution. The following conclusions can be drawn from this study.

- The effect of PTO loading at operational wave conditions, irrespective of the type of loading system (one-way or two-way), the absorbed power is quadratic in behavior. The susceptibility of the absorbed power is low in the one-way τ_{pto} system and strong in the two-way τ_{pto} system.
- As the H_s increases, the average P_{abs} increases rapidly in two-way τ_{pto} and slowly in one-way τ_{pto} , indicating the nonlinear interaction with the complex wave breaking around the WEC-rotor.
- For a fixed τ_{pto} , the pitch RAO increases with the wave period until the wave period reaches to maximum and then decreases. This trend is similar for both the one-way and two-way PTO loading systems. The magnitude of the average absorbed power is higher for the two-way τ_{pto} system than for the one-way τ_{pto} system at a fixed PTO loading within the range of wave periods considered.
- The hydrodynamic behavior of the WEC-rotor at the high sea wave condition of power extraction is similar to that at operational conditions, but the efficiency seems to be lower.
- The flow visualization of the WEC-rotor reveals that the WEC-rotor is associated with higher and stronger wave runup, slamming, and wave breaking under high sea wave conditions than under operational wave conditions.

The present hydrodynamic analysis on the WEC-rotor exposed to irregular wave provides instructive guidance for further performance assessment. In the future, the study will be extended for comparison with the real-time field-testing data.

Acknowledgments

This research was supported by the 2021 scientific promotion program funded by Jeju National University

References

- António, F.D.O. (2007), “Modelling and control of oscillating-body wave energy converters with hydraulic power take-off and gas accumulator”, *Ocean Eng.*, **34**(14-15), 2021-2032. <https://doi.org/10.1016/j.oceaneng.2007.02.006>.
- António, F.D.O. (2008), “Phase control through load control of oscillating-body wave energy converters with hydraulic PTO system”, *Ocean Eng.*, **35**(3-4), 358-366. <https://doi.org/10.1016/j.oceaneng.2007.10.005>.
- Bhattacharyya, R. and McCormick, M.E. (2003), *Wave Energy Conversion*. Elsevier ocean engineering book series, Oxford, UK.
- DNV G. DNV-RP-H103 (2014), *Modelling and Analysis of Marine Operations*. DNV GL.
- Falnes, J. (2002), *Ocean Waves and Oscillating Systems: Linear Interactions including Wave-Energy Extraction*, Cambridge University Press, Cambridge, UK.
- Folley, M. (2016), *Numerical Modelling of Wave Energy Converters: State-of-the-Art Techniques for Single Devices and Arrays*, Academic Press, Cambridge, MA, USA.
- Ha, Y.J., Park, J.Y. and Shin, S.H. (2021), “Numerical study of non-linear dynamic behavior of an asymmetric rotor for wave energy converter in regular waves”, *Processes*, **9**(8), 1477. <https://doi.org/10.3390/pr9081477>.
- Kim, D., Poguluri, S.K., Ko, H.S., Lee, H. and Bae, Y.H. (2019), “Numerical and experimental study on linear behavior of salter's duck wave energy converter”, *J. Ocean Eng. Technol.*, **33**(2), 116-122. <https://doi.org/10.26748/KSOE.2019.023>.
- Ko, H.S., Kim, S. and Bae, Y.H. (2021), “Study on optimum power take-off torque of an asymmetric wave energy converter in Western Sea of Jeju Island”, *Energies*, **14**(5), 1449. <https://doi.org/10.3390/en14051449>.
- Pecher, A. and Kofoed, J.P. (2017), *Handbook of ocean wave energy*. Springer Nature.
- Pecher, A., Kofoed, J.P., Larsen, T. and Marchalot, T. (2012), “Experimental study of the Weptos wave energy converter”, *Proceedings of the 31st International Conference on Ocean, Offshore and Arctic Engineering*, Rio de Janeiro, Brazil, July.
- Peretta, S., Ruol, P., Martinelli, L., Tetu, A. and Kofoed, J.P. (2015), “Effect of a negative stiffness mechanism on the performance of the Weptos rotors”, In *MARINE VI: proceedings of the VI International Conference on Computational Methods in Marine Engineering*, CIMNE.
- Pizer, D. (1994), *Numerical Modelling of Wave Energy Absorbers*. Harwell Laboratory, Energy Technology Support Unit, UK.
- Poguluri, S.K. and Bae, Y.H. (2018), “A study on performance assessment of WEC rotor in the Jeju western waters”, *Ocean Syst. Eng.*, **8**(4), 361-380. <https://doi.org/10.12989/ose.2018.8.4.361>.
- Poguluri, S.K., Cho, I.H. and Bae, Y.H. (2019), “A study of the hydrodynamic performance of a pitch-type wave energy converter-rotor”, *Energies*, **12**(5), 842. <https://doi.org/10.3390/en12050842>.
- Poguluri, S.K., Ko, H.S. and Bae, Y.H. (2020), “CFD investigation of pitch-type wave energy converter-rotor based on RANS simulations”, *Ship. Offshore Struct.*, **15**(10), 1107-1119. <https://doi.org/10.1080/17445302.2019.1705632>.
- Salter, S.H. (1974), “Wave power”, *Nature*, **249**(5459), 720-724.
- Skyner, D. (1987), *Solo Duck Linear Analysis*, University of Edinburgh, Edinburgh, UK.